DOI：10. 11714/acta. snus. ZR20250199

Retrieving the colors of resonance modes in nanophotonic structures: A case study of Gold Nanoplates and Silicon Nanospheres*

Wang Jing[1,2,3], *Li Jincheng*[1,2,3], *Zhu Hongjia*[1,2,3], *Liu Pu*[4], *Shao Lei*[1,2,3], *Chen Huanjun*[1,2,3]✉

1.State Key Laboratory of Optoelectronic Materials and Technologies, Guangzhou 510275, China
2.Guangdong Province Key Lab of Display Material and Technology, Guangzhou 510275, China
3.School of Electronics and Information Technology, Sun Yat-sen University, Guangzhou 510006, China
4.School of Materials Science and Engineering, Sun Yat-sen University, Guangzhou 510006, China

Abstract: The resonance modes in nanophotonic structures, such as plasmonic oscillations in metals and Mie resonances in semiconductors, govern their optical responses. Yet, directly linking these modes to perceptible colors at the single-particle level remains difficult. Here, we investigate gold nanoplates (Au NPs) as plasmonic resonators and silicon nanospheres (Si NSs) as dielectric resonators, and establish a systematic method to retrieve and visualize the colors associated with their resonant modes. Single-particle dark-field scattering spectroscopy was combined with a quantitative conversion framework based on the CIE 1931 color space. Au NPs were synthesized via wet-chemical anisotropic oxidation, and Si NSs by nanosecond laser ablation in liquid, enabling precise tuning of their resonances across the visible spectrum(454~769 nm). Scattering spectra of individual nanoparticles were acquired and converted to CIE tristimulus values and sRGB colors following ASTM E308 standards. Si NSs exhibit broad Mie resonances that produce a diverse color palette, whereas Au NPs support narrower plasmonic resonances that yield highly saturated colors. This work establishes a general framework linking nanoscale resonances to macroscale color perception, providing a guideline for designing nanostructures for applications in displays, imaging, and sensing.

Key words: nanophotonics; structural color; plasmonic resonances; Mie resonances; dark-field scattering; colorimetry; gold nanoplates; silicon nanospheres

CLC number: O47 **Document code:** A **Article ID:** 2097 − 0137(XXXX)XX − 0001 − 09

Nanophotonics, which focuses on controlling light-matter interactions at the nanoscale, is central to the advancement of emerging optical technologies such as sensing(Jain et al.,2006),communication(Sardar et al., 2009),and nano-/micro-display systems. At these dimensions, resonance modes ranging from plasmonic oscillations in metals(Jain et al.,2006;Eustis et al.,2006) to dielectric Mie resonances in semiconductors govern the optical response of nanostructures. These resonances dictate the spectral positions,scattering efficiencies, and near-field distributions that define how nanostructures interact with light. Importantly, retrieving and visualizing the "colors" associated with these modes provides a direct and intuitive link between struc-

* **Received**: 2025−09−15 **Accepted**: 2025−10−15 **Published online**: XXXX−XX−XX
Supported by National Key R&D Program “Frontiers of Nanotechnology” Key Projects（2024YFA1208500，2024YFA1208501）
✉**Corresponding author**：Chen Huanjun(*Chenhj8@mail.sysu.edu.cn*)

Wang Jing（*wangj968@mail. sysu. edu. cn*）；Li Jincheng（*Chenhj8@mail. sysu. edu. cn*）；Zhu Hongjia（*Chenhj8@mail. sysu. edu. cn*）；Liu Pu（*liupu5@mail. sysu. edu. cn*）；Shao Lei（*shaolei5@mail.sysu.edu.cn*）;Chen Huanjun(*Chenhj8@mail.sysu.edu.cn*)

tural resonances and observable optical effects. Such color-based interpretation not only aids in the understanding of fundamental nanophotonic processes but also facilitates the rational design of nanoscale components for optical applications.

Although resonances play a central role in nanophotonic structures, directly linking their properties to perceptible colors remains challenging, particularly at the single-particle level. Resonance modes often overlap and extend across broadband spectra(Child, 1985), making it difficult to disentangle their individual contributions to the observed optical response. Conventional approaches typically rely on far-field spectroscopy of ensembles(Jans et al.,2010; Li et al., 2010) or advanced near-field measurements on single particles (Zhou et al.,2010). While these methods are rigorous, they do not readily translate resonance characteristics into a colorimetric or application-oriented framework. Developing methodologies that connect resonance features with perceptible color signatures can provide a bridge between fundamental nanophotonic physics with practical optical perception, with implications for imaging, display, and sensing technologies.

This work investigates two archetypal nanophotonic systems: Au NPs(as plasmonic resonators) and Si NSs(as dielectric resonators). Au NPs exhibit strong localized surface plasmon resonances(LSPRs), which are highly tunable through geometry and surface chemistry(Min et al., 2020;Qin et al., 2016;Cui et al., 2018). In contrast, Si NSs, owing to their high refractive index, sustain well-defined electric and magnetic multipolar Mie resonances(Palik, 1997;Staude et al., 2013;Kuznetsov et al., 2012). By comparing their optical responses, we establish a general framework for retrieving and visualizing modal colors across different resonance types. The objective of this study is to develop and demonstrate a methodology for retrieving resonance colors from individual nanostructures using dark-field scattering imaging and spectroscopy (Gao et al., 2021). By directly linking spectral information to perceptible colors within the CIE 1931 color space(Ohno, 2000), this approach provides an intuitive visual representation of resonant modes. Such visualization not only complements traditional spectral analysis but also makes the phenomena of nanophotonic resonance more accessible. In addition, this work deepens the understanding of light-matter interactions, guides the design of nanophotonic structures for color generation and display, and offers a nanoscale versatile tool for illustrating structural color phenomena in applied optics(Yang et al., 2019).

1 Sample preparation

The Si NSs with various diameters were synthesized using nanosecond laser ablation in liquid (LAL). LAL technique is widely recognized as an efficient method for producing ultra-pure nanoparticle colloids(Kuznetsov et al., 2012; Evlyukhin et al., 2012). During the experiment, 10 mg of high-purity silicon powder was dispersed and ultrasonicated in a 50 mL mixed solution of water and isopropanol . The volume ratio of water to isopropanol is 1:3. A single-crystalline silicon wafer was used as a protective substrate and immersed in the solution. An ultrafast nanosecond pulsed Nd: YAG laser served as the ablation source, with operating parameters of 532 nm wavelength, 10 ns pulse width, 10 Hz repetition frequency, and 500 mJ pulse energy. The laser beam was focused onto the suspension by a 500 mm focal length lens, and continuous ablation for 1 h yielded a colloidal solution of Si NSs with a broad size distribution, where the Si NSs range in 200~1 000 nm.

As shown in Fig. 1b, the SEM image confirms that the as-grown Si NSs possess a nearly spherical morphology with smooth surfaces. This indicates that the surface energy is minimized during the rapid cooling process in the liquid phase. The particle diameters range from several tens to a few hundred nanometers, reflecting the inherent polydispersity of the LAL method. Larger spheres are likely formed through coalescence of smaller molten droplets, while the presence of smaller particles suggests incomplete aggregation during the ablation process. The dispersion of size and shape is crucial, as it directly influences the variation of optical resonances and colorimetric properties investigated in this work.

The synthesis of circular Au NPs was achieved through a well-controlled anisotropic oxidation process of pre-formed triangular Au NPs(Qin et al., 2016; Cui et al., 2018), as illustrated in Fig. 1b. Triangular Au NPs were synthesized via a seed-mediated growth method(Fig.1c). Briefly,an aqueous solution of $HAuCl_4$

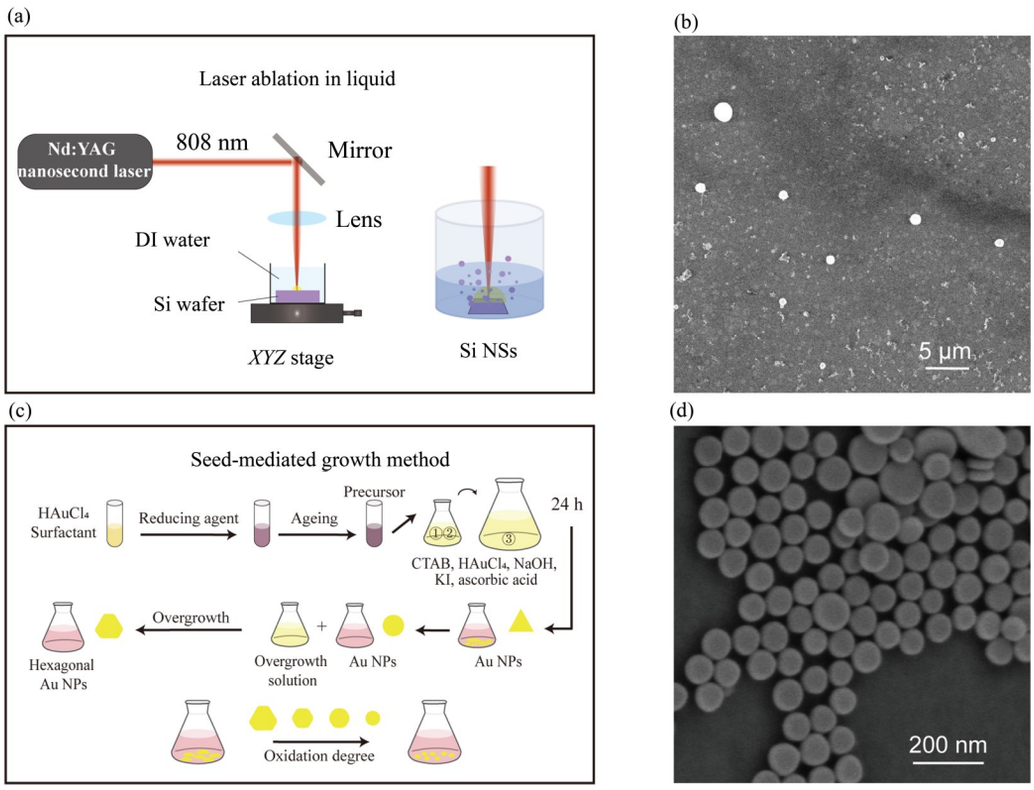

Fig. 1 Synthesis of silicon nanospheres (Si NSs) and gold nanoplates (Au NPs)

was mixed with a solution of cetyltrimethylammonium bromide(CTAB), which acted as a stabilizing and structure-directing agent. Under vigorous stirring, an ice-cold $NaBH_4$ solution was added to rapidly reduce Au^{3+} ions and generate gold seeds. The resulting seed solution was then aged for 2~6 h to allow complete hydrolysis of any unreacted $NaBH_4$. Concurrently, three growth solutions(denoted as ①,②,③) with identical compositions but different volumes were prepared. Each growth solution contained CTAB, $HAuCl_4$, KI, sodium hydroxide(NaOH), and ascorbic acid. The role of KI and NaOH is to promote anisotropic growth by selective adsorption on specific crystal facets. A portion of the seed solution was sequentially introduced to growth solutions ①, ②, ③, with gentle shaking after each addition to ensure mixing. After each step, a portion of the mixture was transferred to the next growth solution. The final combined mixture was left undisturbed at room temperature for 24 h, enabling the synthesized triangular Au NPs to precipitate to the bottom of the reaction vessel via depletion-induced self-precipitation.

The triangular Au NPs synthesized above will automatically become circular in water. Overgrowth solutions were prepared, each containing CTAB, $HAuCl_4$, ascorbic acid, and water. The circular Au NPs solution was introduced into each overgrowth solution, and the reaction was conducted in an isothermal oven at 30 °C for 10 h (Fig. 1b). The thickness of the Au NPs will increase with the increasing in the amount of $HAuCl_4$, while the lateral dimensions remain almost unchanged. The anisotropic oxidation was then initiated at room temperature by introducing a mixture of H_2O_2 and HCl into the NP solution(Jang et al. , 2014). H_2O_2 is used as an oxidizer because it's easy to handle and the reaction conditions are mild, while HCl was used to modulate the oxidation rate by controlling the concentration of H^+ ions. This process, depicted from left to right in the bottom row of Fig. 1b, involves the gradual rounding of the sharp corners and the subsequent reduction in the diameter of the NPs, ultimately yielding circular NPs. The progression of the reaction was monitored by the visible color change of the solution. By precisely terminating the oxidation at different time points through centrifugation, a series of monodisperse circular Au NPs with continuously tunable diameters ranging from approximately 150 nm to 50 nm could be obtained,

while maintaining a constant thickness of 35 nm inherited from the initial NPs.

2 Principle of color retrieving from the single-particle dark-field scattering spectroscopy

As shown in Fig. 1b, the scattering images and spectra of individual Au NPs and Si NSs were collected using a dark-field optical microscope (Princeton Instrument Action SP2300) equipped with a quartz tungsten-halogen lamp (100 W) and a charge-coupled device (CCD) camera (Princeton Instruments Pixis 400BR_eXcelon). The CCD was cooled to −70 °C during the measurements to reduce noise. A dark-field objective (100×, NA = 0. 80) was used to illuminate specific nanostructures with white excitation light and collect their scattered signals. To obtain accurate scattering spectra, background signals were first recorded from adjacent regions without nanostructures and subtracted, followed by correction with the calibrated response curve of the optical system. Color scattering images were acquired with a digital camera(ARTCAM300MIC) mounted at the imaging plane of the microscope.

In dark-field optical microscopy, a bright image of the nanostructure is formed against a dark background, which effectively suppresses unwanted reflection from the substrate. This is achieved by inserting an opaque disc between the light source and condenser lens, which blocks the direct illumination path (Fig. 2). As a result, the light reaching the sample is shaped into a hollow cone that strikes the nanostructure at a large incident angle. Only light that is scattered, refracted, or reflected by the nanostructure would enter into the objective lens, while unscattered light pass it. Consequently, background reflections are largely excluded, and the nanostructure itself appears as a bright, well-resolved feature on a dark field of view. This configuration enables clear visualization and quantitative spectroscopy of individual nanoparticles while minimizing interference from the substrate or surrounding medium.

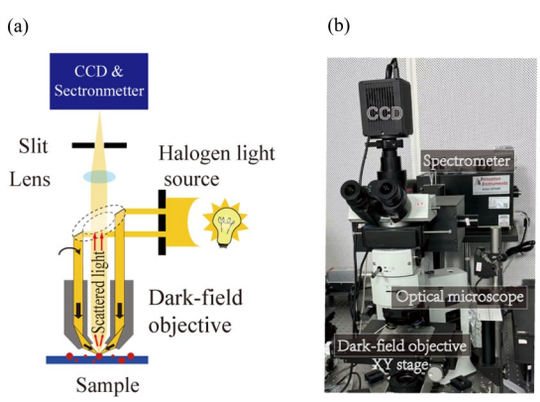

Fig. 2 The custom dark-field microscopy

After obtaining the scattering spectrum and dark-field image of an individual nanostructure, its spectral response can be quantitatively correlated with the perceived color captured in the dark-field image. This process involves several transformation steps. First, the measured scattering spectrum is converted into CIE tristimulus values(X, Y, Z)(Billmeyer et al., 1987). These tristimulus values are then normalized to chromaticity coordinates(x, y, z)(Loesdau et al., 2017). Next,the chromaticity values are mapped to an RGB color space, and finally the normalized RGB values (ranging from 0 to 1) are scaled into 8 bit values (0~255) for visualization. To determine the tristimulus values (X, Y, Z) from a given visible-light spectrum, the spectrum is weighted against the standard CIE color matching functions(Wyman et al. , 2013)(Supply:Appendix Fig. 2). For example, Supply: Appendix Fig. 1 shows the visible spectrum of potassium permanganate,which can be projected onto the CIE functions to yield corresponding X,Y,Z values. This procedure is described in detail in ASTM E308(Wyszecki et al., 2000), which specifies how to transform spectral data into CIE tristimulus values. A practical consideration is that measured spectra often have sub-nanometer resolution, whereas the CIE 1931 standard observer functions are tabulated at 5-nm intervals between 400 and 700 nm. Therefore, the raw spectral data should be resampled or averaged to 5-nm intervals before integration.

For a given emissive power distribution, $P(\lambda)$, from an individual nanostructure,the X,Y,Z tristimulus values are computed as,

$$X = \int \bar{x}(\lambda)P(\lambda)\mathrm{d}\lambda,\quad Y = \int \bar{y}(\lambda)P(\lambda)\mathrm{d}\lambda,\quad Z = \int \bar{z}(\lambda)P(\lambda)\mathrm{d}\lambda,$$

$\bar{x}$, $\bar{y}$ and $\bar{z}$ denote the CIE standard observer color-matching functions (available for either the 2° or 10° field of view, depending on the application). In our study, we applied the values obtained at 10° field of

view, because the incident angle of the dark-field objective is over 50°. The integrals are evaluated over the visible range 360~830 nm, where the standard observer functions are nonzero. In practice, the measured spectral power distribution(SPD) may cover a narrower wavelength range, depending on the characteristics of the measuring instrument(Farup et al., 2007). The spectral sampling interval is typically between 1~20 nm. To ensure accurate calculation of the tristimulus values, the wavelength range and spacing of the SPD must be matched to those of the standard observer functions. This alignment is achieved through resampling, interpolation, and, if necessary,extrapolation of the measured data.

Cases involving reflective and transmissive samples share similarities with, but also differ from, the emissive case described earlier. In these cases, the spectral power distribution of the sample, $P(\lambda)$ is replaced by the product of the sample's spectral reflectance (or transmittance), $S(\lambda)$, and the spectral power distribution of a reference illuminant, $I(\lambda)$,

$$X = \frac{1}{N}\int \bar{x}(\lambda)S(\lambda)I(\lambda)\mathrm{d}\lambda,$$
$$Y = \frac{1}{N}\int \bar{y}(\lambda)S(\lambda)I(\lambda)\mathrm{d}\lambda,$$
$$Z = \frac{1}{N}\int \bar{z}(\lambda)S(\lambda)I(\lambda)\mathrm{d}\lambda,$$

with the normalization constant, $N = \int \bar{y}(\lambda)I(\lambda)\mathrm{d}\lambda$. Once the tristimulus values $[X,Y,Z]$ are determined, they can be converted to chromaticity coordinates,

$$x = X/(X+Y+Z),\quad y = Y/(X+Y+Z),\quad z = Z/(X+Y+Z).$$

Since $x+y+z=1$, only (x,y) are needed to plot the color on the CIE chromaticity diagram. A special case occurs for black, where $X=Y=Z=0$. In this situation, (x,y) are undefined, and it is common to assign the chromaticity of the reference white as a fallback. The transformation from tristimulus values $[X,Y,Z]$ to RGB values makes use of a linear matrix transformation as

$$\begin{bmatrix} X \\ Y \\ Z \end{bmatrix} = \boldsymbol{M}\begin{bmatrix} R \\ G \\ B \end{bmatrix},$$

where the transformation matrix $\boldsymbol{M}$ is calculated from the RGB system's chromaticity coordinates and its reference white point. Specifically, given the chromaticity coordinates of the RGB primaries $(x_\mathrm{r}, y_\mathrm{r}), (x_\mathrm{g}, y_\mathrm{g}), (x_\mathrm{b}, y_\mathrm{b})$ and the reference white point $(X_\mathrm{W}, Y_\mathrm{W}, Z_\mathrm{W})$, a 3×3 matrix can be derived to convert between RGB and XYZ spaces according to the following algorithm,

$$\boldsymbol{M} = \begin{bmatrix} S_\mathrm{r}X_\mathrm{r} & S_\mathrm{g}X_\mathrm{g} & S_\mathrm{b}X_\mathrm{b} \\ S_\mathrm{r}Y_\mathrm{r} & S_\mathrm{g}Y_\mathrm{g} & S_\mathrm{b}Y_\mathrm{b} \\ S_\mathrm{r}Z_\mathrm{r} & S_\mathrm{g}Z_\mathrm{g} & S_\mathrm{b}Z_\mathrm{b} \end{bmatrix},$$
$$X_\mathrm{r} = x_\mathrm{r}/y_\mathrm{r},\quad Y_\mathrm{r} = 1,\quad Z_\mathrm{r} = (1-x_\mathrm{r}-y_\mathrm{r}),$$
$$X_\mathrm{g} = x_\mathrm{g}/y_\mathrm{g},\quad Y_\mathrm{g} = 1,\quad Z_\mathrm{g} = (1-x_\mathrm{g}-y_\mathrm{g})/y_\mathrm{g},$$
$$X_\mathrm{b} = x_\mathrm{b}/y_\mathrm{b},\quad Y_\mathrm{b} = 1,\quad Z_\mathrm{b} = (1-x_\mathrm{b}-y_\mathrm{b})/y_\mathrm{b},$$
$$\begin{bmatrix} X_\mathrm{W} \\ Y_\mathrm{W} \\ Z_\mathrm{W} \end{bmatrix} = \begin{bmatrix} X_\mathrm{r} & X_\mathrm{r} & X_\mathrm{b} \\ Y_\mathrm{r} & Y_\mathrm{r} & Y_\mathrm{b} \\ Z_\mathrm{r} & Z_\mathrm{g} & Z_\mathrm{b} \end{bmatrix}\begin{bmatrix} S_\mathrm{r} \\ S_\mathrm{g} \\ S_\mathrm{b} \end{bmatrix}.$$

The final step is to convert the normalized RGB values into 8-bit values, as is standard in digital imaging. In most computer graphics systems, each color channel (R,G,B) is represented with 8 bits. This corresponds to integer values ranging from 0 to 255, where [0, 0, 0] represents black and [255] represents white. To achieve this, the normalized RGB values, ranging from 0 to 1, are scaled by 255 and rounded to the nearest integer. Values outside the valid range are clipped using a conditional statement, for example,

$$R_{8-\mathrm{bit}} = \begin{cases} 0, & sR < 0; \\ 255, & sR > 1; \\ \mathrm{round}(sR \times 255), & \text{otherwise.} \end{cases}$$

The same operation is applied to G and B. The resulting integer values $[R_{8\text{-bit}}, G_{8\text{-bit}}, B_{8\text{-bit}}]$ can then be directly used to render the corresponding perceptible color on digital displays or in colorimetric visualization. In summary, the visible scattering spectrum obtained from dark-field measurements can be quantitatively transformed into perceptible color using the framework of the CIE 1931 chromaticity system(Fig. 3). By applying the standard color matching functions and following the procedures outlined in ASTM E308, the spectral data are converted into tristimulus values $[X,Y,Z]$, which then be mapped into the RGB color space and finally encoded into 8-bit color values for visualization. This workflow bridges the gap between nanoscale optical responses and macroscale color perception, enabling intuitively interpreting the resonant scattering properties of plasmonic and dielectric nanostructures. In doing so, it provides a direct means of visualizing how structural colors arise from physical spectra, offering valuable insights for both fundamental material studies and applied nanophotonic design.

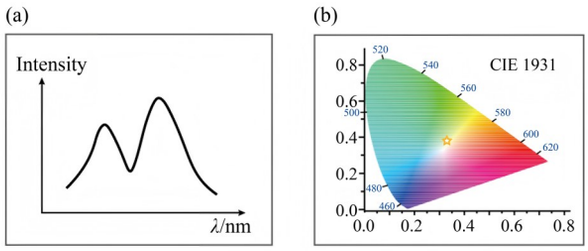

Fig. 3 The visible scattering spectrum obtained from dark-field measurement

3 Dark-field imaging and spectroscopy characterizations

The as-grown Au NPs and Si NSs were immobilized onto a silicon substrate covered by a 300-nm-thick silicon dioxide layer for dark-field scattering imaging and spectroscopy. A pattern-matching method(Kunetsov et al., 2012) was used to correlate the positions of individual nanostructures between SEM and dark-field scattering images (Fig. 4). The scattering spectra were then acquired from single nanostructures using the dark-field setup illustrated in Fig. 2b. Fig. 4a presents results for three representative Au NPs. Their scattering spectra are characterized by broad resonances in the visible range, arising from LSPRs(Qin et al., 2016; Cui et al., 2018; Mayer et al., 2011). The spectral position of these resonances is highly sensitive to particle size. Specifically, as the nanoparticle diameter increases from 84 nm to 134 nm, the scattering maximum redshifts from 560 nm to 620 nm. This size-dependent redshift is a hallmark of plasmonic behavior, reflecting the longer oscillation period of the collective electron cloud in larger particles, agreeing well with numerical finite-difference time-domain (FDTD) simulations (Supply: Appendix Fig. 3a) The influence of LSPRs on color appearance is directly evident in the dark-field images. The NP with a resonance peak near 560 nm appears light green, while the NP with a resonance shifted to 620 nm exhibits a red hue. Thus, subtle variations in nanoparticle size translate into perceptible color differences, highlighting the intrinsic link between nanoscale plasmonic resonances and macroscale optical appearance.

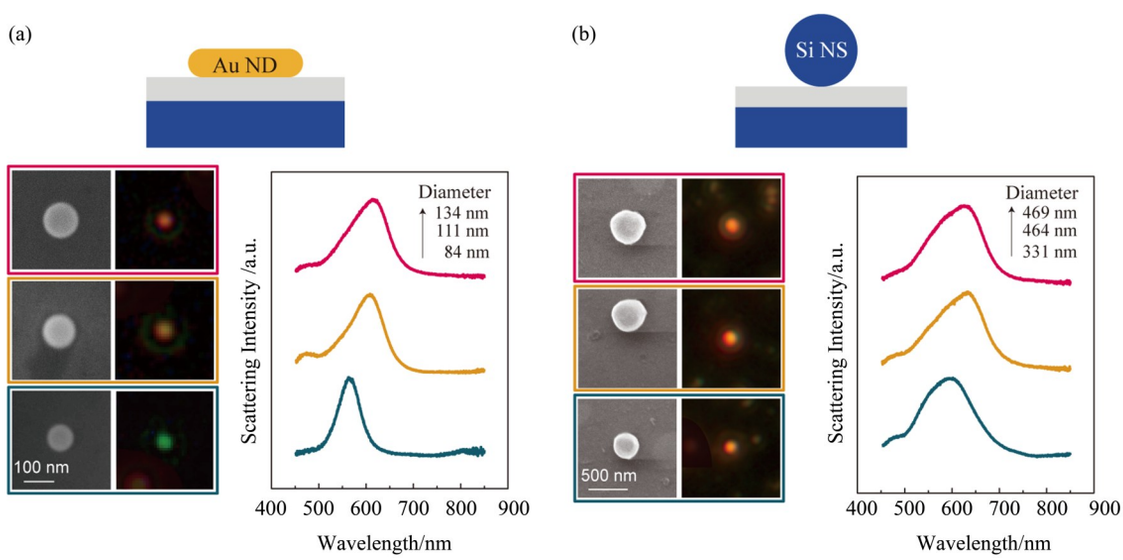

Fig. 4 Dark-field imaging and spectroscopy characterizations of gold nanoplates and silicon nanospheres

In contrast, Fig. 4b shows results for Si NSs. Unlike metals, dielectric nanospheres support well-defined multipolar Mie resonances due to their high refractive index(Mie, 1908; Decker et al., 2016; Yao et al., 2023). For the sizes studied here, the dominant mode in the visible regime is the magnetic dipolar or high-order mode resonance(Kuznetsov et al., 2012; Jang et al., 2014; Decker et al., 2016). As the Si NS diameter increases from 331 nm to 469 nm, the magnetic dipole resonance undergoes a redshift from ~480 nm to ~580 nm. Such spectral evolution was further corroborated by FDTD simulations (Supply: Appendix Fig. 3b). This shift produces an evolution in perceived color, with smaller spheres appearing orange and

larger spheres exhibiting more yellow hues in dark-field images. It should be noticed that the narrow and well-resolved nature of the LSPRs in Au NPs contrasts with the broader Mie resonance peaks of Si NSs, leading to sharper color transitions (Fig. 4). Taken together, these results highlight two distinct mechanisms for structural coloration at the nanoscale. In metals such as Au, color arises from collective oscillations of free electrons, which produce relatively narrow scattering with size-tunable peaks(Rash et al., 2009). In high-index dielectrics such as Si, color originates from Mie resonances,in particular magnetic dipolar modes, which are dictated by geometric confinement of displacement currents(Evlyukhin et al.,2012;Rasch et al.,2009;Garcia-Etxarri et al.,2011; Sugimoto et al., 2020). While different in physical origin — one rooted in free-electron dynamics and the other in dielectric wave confinement — both mechanisms critically determine how a nanoparticle's optical resonances map onto human-perceivable colors. This underscores the universality of resonance-driven structural coloration in nanophotonics and its utility for applications ranging from display technologies to optical sensing.

4 Retrieving the colors from the single-particle scattering spectra

To quantitatively connect the resonant scattering of individual nanoparticles with their perceptible colors, we applied the colorimetric conversion formalism described in Section 3. Each measured scattering spectrum $S(\lambda)$ was treated as a spectral power distribution and combined with the CIE 1931 standard observer functions under the D65 illuminant. From this, the CIE XYZ tristimulus values were obtained, converted into chromaticity coordinates(x,y), and then transformed into standard sRGB values for digital visualization. This procedure enables a direct comparison between the retrieved colors and the hues observed in dark-field scattering images.

For the Au NPs, the retrieved colors showed excellent agreement with experimental observations. For example, an NP with a scattering peak at 580 nm (Fig. 4a) yielded a light green hue (sRGB≈[173,220, 114]), consistent with its appearance in microscopy (Fig.4a, bottom panel). As the NP diameter increased and the resonance redshifted to 620 nm,the retrieved color transitioned to a saturated red (sRGB≈[215,75, 57]). Importantly, the narrow linewidth of the LSPR peaks contributed to high color saturation, which the formalism accurately captured, yielding vivid and well-defined hues (Fig. 4a, upper panel). The same procedure applied to Si NSs confirmed its robustness for dielectric systems (Fig.4b). A smaller Si NS with a magnetic dipole resonance near 480 nm produced an orange color (sRGB≈ [240, 150, 70]), while a larger sphere resonating near 580 nm appeared yellow (sRGB≈[230,200,60]). Unlike plasmonic resonances, the Mie resonances in Si NSs are typically broader and spectrally overlapping. Despite this,the retrieved colors closely matched the dark-field image (Fig. 4b, lower panel), demonstrating that the method can faithfully translate even less spectrally sharp features into perceptible colors. The results highlight the differing physical origins of color in plasmonic and dielectric nanostructures — arising from collective free-electron oscillations in Au NPs and from high-index Mie resonances in Si NSs — while showing that both can be mapped onto a common perceptual framework.

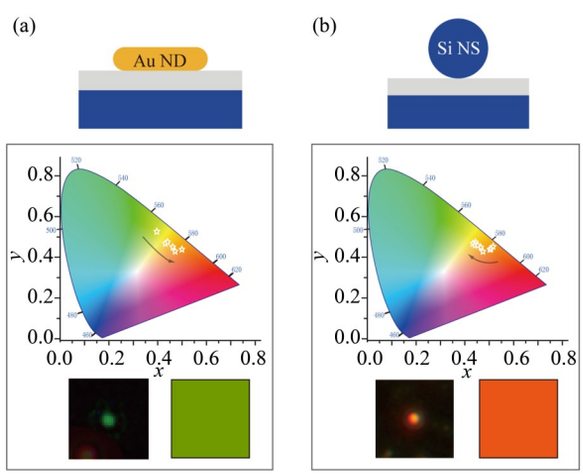

Fig. 4 Comparison of experimental dark-field images and retrieved colors of individual nanoparticles

Overall, the color retrieval formalism proved effective in translating scattering spectra into accurate visual colors for both plasmonic and dielectric resonators. The close match between computed sRGB values and microscopy scattering images confirms the efficacy and universality of this approach for

nanophotonic color interpretation. Beyond validation, this framework provides a quantitative bridge between nanoscale resonance physics and human color perception,enabling researchers to intuitively visualize how structural colors emerge from physical spectra. Future refinements could include more rigorous instrument-response calibration, improved angular collection to better approximate the CIE standard observer, and adoption of advanced color appearance models(e. g. CIECAM02) to account for perceptual differences under varying illumination and viewing conditions(Moroney et al.,2002;Luo et al.,2006).

5 Conclusion

We established a systematic approach for quantifying and visualizing the structural colors of plasmonic and dielectric nanostructures using dark-field scattering spectroscopy combined with CIE 1931 color space conversion. Au NPs were synthesized via a wet-chemistry route, and Si NSs were produced by laser ablation, enabling precise control of their resonant properties and tunable scattering colors across the visible range (454~769 nm). Dark-field microscopy,integrated with calibrated spectral analysis, allowed us to capture the scattering response of individual nanoparticles. The subsequent application of CIE standard observer functions and ASTM E308 protocols transformed these spectra into perceptible RGB colors with high fidelity. A direct comparison between the two systems highlights the different physical origins of their colors: Au NPs exhibit localized surface plasmon resonances,yielding tunable narrow spectra that produce rich and saturated colors,whereas Si NSs support Mie resonances arising from their high refractive index, leading to broad and dynamic hues. This contrast underscores the complementary roles of plasmonic and dielectric resonances in structural color generation. Overall,this framework bridges nanoscale resonance phenomena with macroscale color perception, providing a versatile tool for the rational design of nanostructures in displays, imaging, and sensing.

Reference:

Billmeyer Jr F W, Fairman H S, 1987. CIE method for calculating tristimulus values[J].Color Res Appl, 12(1): 27-36.

Bottema M, 2011. Digital image computing techniques and applications (DICTA) conference 2009 [J]. IET Comput Vis, 5(4): 191.

Child M S, 1985. Local mode overtone spectra[J]. Acc Chem Res, 18(2): 45-50.

Cui X M, Qin F, Ruan Q F, et al, 2018. Circular gold nanodisks with synthetically tunable diameters and thicknesses[J]. Adv Funct Mater, 28(11): 1705516.

Decker M, Staude I, 2016. Resonant dielectric nanostructures: A low-loss platform for functional nanophotonics [J]. J Opt, 18(10): 103001.

Eustis S, EI-Sayed M A, 2006. Why gold nanoparticles are more precious than pretty gold: Noble metal surface plasmon resonance and its enhancement of the radiative and nonradiative properties of nanocrystals of different shapes[J]. Chem Soc Rev, 35(3): 209-217.

Evlyukhin A B, Novikov S M, Zywietz U, et al, 2012. Demonstration of magnetic dipole resonances of dielectric nanospheres in the visible region[J].Nano Lett, 12(7): 3749-3755.

Farup I, Wold J H, Seim T, et al, 2007. Generating light with a specified spectral power distribution[J]. Appl Opt, 46 (13): 2411.

Gao P F, Lei G, Huang C Z, 2021. Dark-field microscopy: Recent advances in accurate analysis and emerging applications[J]. Anal Chem, 93(11): 4707-4726.

García-Etxarri A, Gómez-Medina R, Froufe-Pérez L S, et al, 2011. Strong magnetic response of submicron Silicon particles in the infrared[J]. Opt Express, 19(6): 4815.

Jain P K, Lee K S, EI-Sayed I H, et al, 2006. Calculated absorption and scattering properties of gold nanoparticles of different size, shape, and composition: Applications in biological imaging and biomedicine[J]. J Phys Chem B, 110(14): 7238-7248.

Jang H J, Ham S, Acapulco Jr J A I, et al, 2014. Fabrication of 2D Au nanorings with Pt framework[J]. J Am Chem Soc, 136(50): 17674-17680.

Jans H, Jans K, Lagae L, et al, 2010. Poly (acrylic acid) -stabilized colloidal gold nanoparticles: Synthesis and properties[J]. Nanotechnology, 21(45): 455702.

Kuznetsov A I, Miroshnichenko A E, Fu Y H, et al, 2012. Magnetic light[J]. Sci Rep, 2: 492.

Loesdau M, Chabrier S, Gabillon A, 2014. Hue and saturation in the RGB color space[C]// Image and Signal Processing. Cham: Springer International Publishing: 203-212.

Loesdau M, Chabrier S, Gabillon A, 2017. Chromatic indices in the normalized rgb color space[C]//2017 International Conference on Digital Image Computing: Techniques and Applications. Sydney, NSW, Australia:1-8.

Luo M R, Cui G, Li C, 2006. Uniform colour spaces based on CIECAM02 colour appearance model [J]. Color Res Appl, 31(4): 320-330.

Mayer K M, Hafner J H, 2011. Localized surface plasmon resonance sensors[J]. Chem Rev, 111(6):3828-3857.

Mie G, 1908. Beiträge zur Optik trüber Medien, speziell kolloidaler Metallösungen [J]. Ann Der Phys, 330 (3): 377-445.

Min Y, Wang Y, 2020. Manipulating bimetallic nanostructures with tunable localized surface plasmon resonance and their applications for sensing[J]. Front Chem, 8:411.

Moroney N, Fairchild M, Hunt R, et al, 2002. The CIECAM02 color appearance model//Proceedings of the Color and Imaging Conference. Society for Imaging Science and Technology. Scottsdale, AZ, USA:23-27.

Ohno Y, 2000. CIE fundamentals for color measurements[J]. Print4fab, 16(1):540-545.

Palik E D, 1997. Handbook of Optical Constants of Solids [M]. Boston: Academic Press.

Qin F, Zhao T, Jiang R, et al, 2016. Thickness control produces gold nanoplates with their plasmon in the visible and near-infrared regions[J]. Adv Opt Mater, 4(1):76-85.

Rasch M R, Sokolov K V, Korgel B A, 2009. Limitations on the optical tunability of small diameter gold nanoshells [J]. Langmuir, 25(19):11777-11785.

Sardar R, Funston A M, Mulvaney P, et al, 2009. Gold nanoparticles: Past, present, and future [J]. Langmuir, 25(24):13840-13851.

Staude I, Miroshnichenko A E, Decker M, et al, 2013. Tailoring directional scattering through magnetic and electric resonances in subwavelength silicon nanodisks [J]. ACS Nano, 7(9):7824-7832.

Sugimoto H, Okazaki T, Fujii M, 2020. Mie resonator color inks of monodispersed and perfectly spherical crystalline silicon nanoparticles[J].Adv Opt Mater, 8(12):2000033.

Wyman C, Sloan P P, Shirley P, 2013. Simple analytic approximations to the CIE XYZ color matching functions [J]. J Comp Graph Tech, 2:1-11.

Wyszecki G, Stiles W S, 2000. Color science: Concepts and methods, quantitative data and formulae Vol. 40 [M]. NewYork, USA: John Wiley & Sons.

Yao X, Hong X, Liu Y, 2023. Visible Mie resonances in dielectric hollow spheres: Principle, regulation, and applications[J]. Responsive Mater, 1(2):e20230019.

Yang B, Cheng H, Chen S, et al, 2019. Structural colors in metasurfaces: Principle, design and applications [J]. Mater Chem Front, 3(5):750-761.

Zhou X, Xu W, Liu G, et al, 2010. Size-dependent catalytic activity and dynamics of gold nanoparticles at the single-molecule level[J]. J Am Chem Soc, 132(1):138-146.

在纳米光子结构中获取共振模式的颜色：以金纳米板和硅纳米球为例

王晶[1,2,3]，李锦城[1,2,3]，朱鸿嘉[1,2,3]，刘璞[4]，邵磊[1,2,3]，陈焕君[1,2,3]

1. 光电材料与技术国家重点实验室，广东 广州 510275
2. 广东省显示材料与技术重点实验室，广东 广州 510275
3. 中山大学电子与信息工程学院，广东 广州 510006
4. 中山大学材料科学与工程学院，广东 广州 510006

摘　要：本文研究了作为等离子体共振器的金纳米板（Au NPs）和作为介电共振器的硅纳米球（Si NSs），并建立了一种系统的方法来获取和可视化与其共振模式对应的颜色。首先，通过湿化学各向异性氧化法合成 Au NPs。然后，通过液体中的纳秒激光烧蚀法制备 Si NSs。最后，将单颗粒暗场散射光谱与基于 CIE 1931 色彩空间的定量转换框架结合，实现了 Au NPs 和 Si NSs 在可见光谱（454~769 nm）范围内共振的精确调控。单个纳米颗粒的散射光谱被获取并按照 ASTM E308 标准转换为 CIE 三刺激值和 sRGB 颜色。结果表明，硅纳米球表现出宽泛的 Mie 共振，从而产生多样的色彩；而金纳米颗粒则支持较窄的等离子体共振，呈现出高度饱和的颜色。这项工作建立了一个将纳米尺度共振与宏观颜色感知联系起来的通用框架，为设计用于显示、成像和传感的纳米结构提供了指南。

关键词：纳米光子学；结构色；等离子体共振；Mie　共振；暗场散射；色度测量；金纳米片；硅纳米球

（责任编辑　王海蓉）